Supporting Information

Analysis of the Performance of Narrow-Bandgap Organic Solar Cells Based on a Diketopyrrolopyrrole Polymer and a Nonfullerene Acceptor

Tom P. A. van der Pol,[1] Junyu Li,[1] Bas T. van Gorkom,[1] Fallon J. M. Colberts,[2] Martijn M. Wienk,[1] René A. J. Janssen[1,3]*

[1] Molecular Materials and Nanosystems & Institute for Complex Molecular Systems, Eindhoven University of Technology, 5600 MB Eindhoven, The Netherlands

[2] Energy Engineering, Zuyd University of Applied Sciences, Nieuw Eyckholt 300, Heerlen 6419 DJ, The Netherlands

[3] Dutch Institute for Fundamental Energy Research, 5612 AJ Eindhoven, The Netherlands

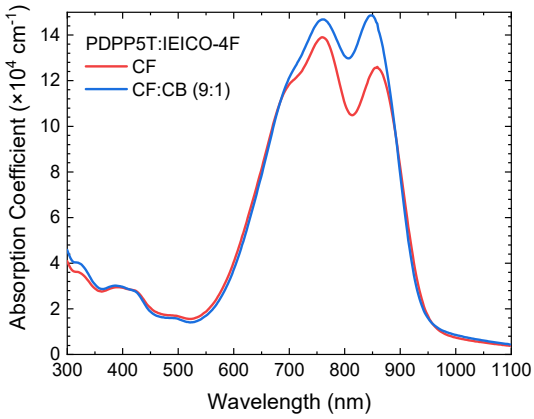

Figure S1. Absorption coefficient spectra of the PDPP5T:IEICO-4F blends (1:2 w/w) cast from CF and CF:CB (9:1).

Table S1. Device statistics for best performing inverted PDPP5T:IEICO-4F solar cells from *J-V* measurements listing averages and standard deviations.

CB (vol %)	J_{SC} (mA cm^{-2})	V_{OC} (V)	FF (-)	PCE (%)
0 [a]	10.2 ± 0.55	0.61 ± 0.005	0.58 ± 0.012	3.6 ± 0.23
1[b]	13.7 ± 0.30	0.57 ± 0.001	0.55 ± 0.018	4.3 ± 0.06
3 [b]	16.1 ± 0.00	0.56 ± 0.002	0.54 ± 0.009	4.9 ± 0.10
5 [c]	15.7 ± 0.20	0.55 ± 0.002	0.50 ± 0.004	4.3 ± 0.04
10 [d]	16.1 ± 0.48	0.54 ± 0.002	0.51 ± 0.007	4.5 ± 0.13

Device statistics based on [a] 8 devices, [b] 2 devices, [c] 4 devices and [d] 12 devices.

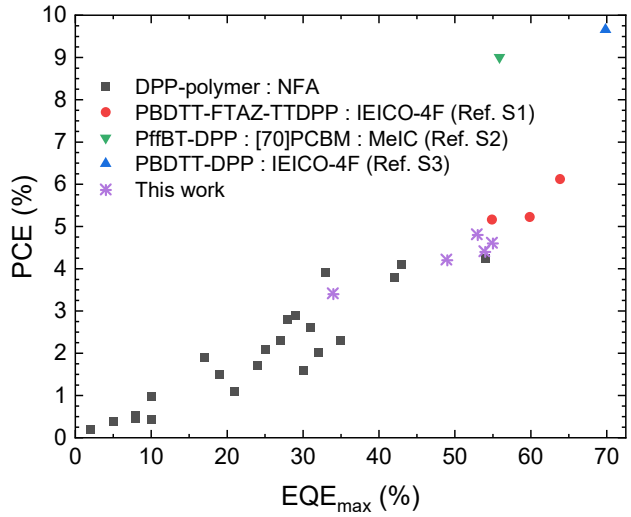

Figure S2. The PCEs and maximum EQEs of solar cells from DPP-containing polymers blended with NFAs reported in the literature and in this work. Highlighted with colors are the random terpolymer based work by Negash *et al.*,[S1] the ternary blend solar cell by Pan *et al.*,[S2] and the current DPP-polymer:NFA record efficiency by Song *et al.*[S3] Other data are from References S4-S11.

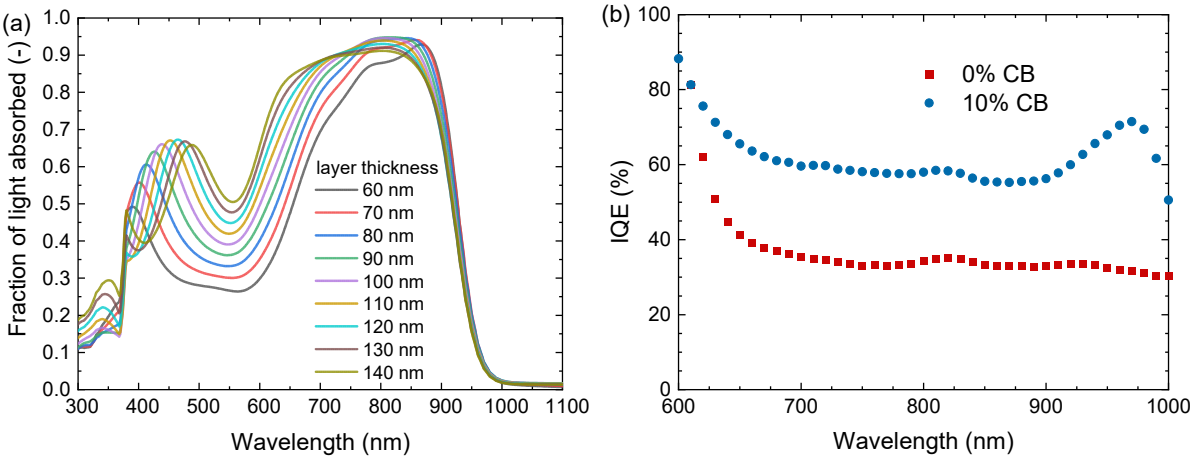

Figure S3. (a) Fraction of light absorbed for different active layer thicknesses as calculated using the transfer matrix formalism incorporated in an in-house script based on the work of Burkhard *et al.*[S12] The simulated device stack consisted of glass/ITO (120 nm)/ZnO (40 nm)/active layer (*x* nm)/MoO_3 (10 nm)/Ag (100 nm). (b) IQE calculated from the EQEs in Figure 2b and the fraction of absorbed light, obtained using the in-house script. The device stack consisted of glass/ITO (120 nm)/ZnO (40 nm)/active layer (130 nm)/MoO_3 (10 nm)/Ag (100 nm) and active layer refractive index data were taken from Figure S10c.

Table S2. Device characteristics for inverted PDPP5T:IEICO-4F solar cells cast from CF:CB (9:1) averaged over two devices except for D:A 1:2 which was averaged over 12 devices.

D:A (w/w)	J_{SC} (mA cm^{-2})	V_{OC} (V)	FF (-)	PCE (%)
1:1	15.0	0.56	0.44	3.7
1:1.5	16.2	0.55	0.50	4.4
1:2	16.1	0.54	0.51	4.5
1:3	15.1	0.55	0.51	4.2

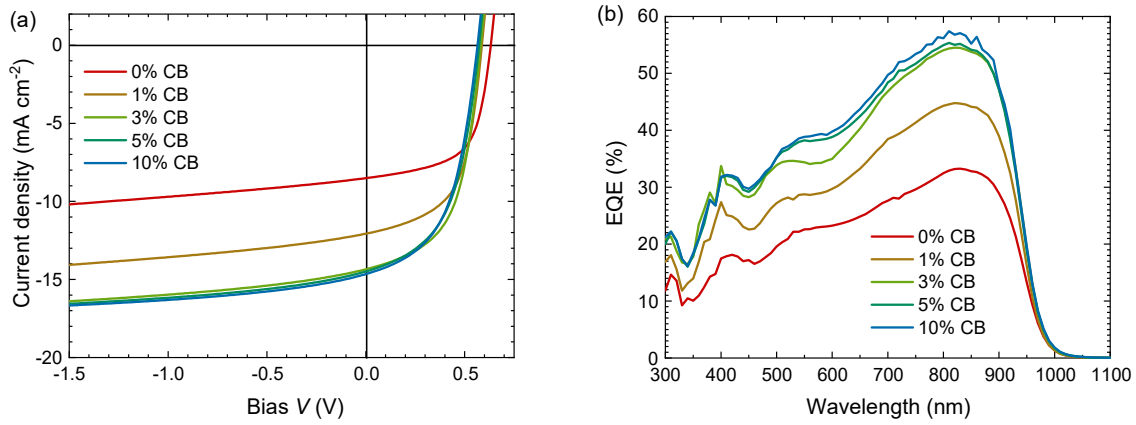

Figure S4. (a) *J*–*V* measurements under simulated AM1.5 G (100 mW cm^{-2}) illumination of inverted PDPP5T:IEICO-4F solar cells cast from CF containing 0, 1, 3, 5, or 10 vol % CB and 0.2 vol % DIO. Film thickness is ~95 nm. (b) Corresponding EQE spectra measured with bias illumination.

Table S3. Device characteristics for PDPP5T:IEICO-4F (95 nm) solar cells cast from CF:CB mixtures.

CB (vol %)	J_{SC} (mA cm^{-2}) [a]	V_{OC}(V)	FF (-)	PCE (%) [a]
0	9.1	0.63	0.61	3.5
1	12.3	0.59	0.58	4.2
3	15.0	0.58	0.55	4.8
5	15.5	0.57	0.52	4.6
10	15.9	0.57	0.52	4.7

[a] J_{SC} determined by integrating the EQE spectrum measured with ~1-sun bias illumination (Figure S4b).

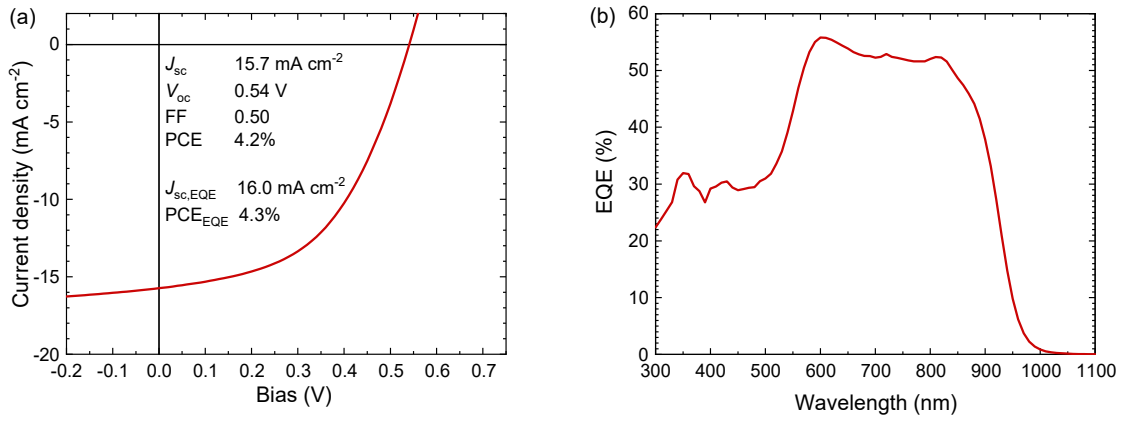

Figure S5. (a) *J*–*V* measurements under simulated AM1.5 G (100 mW cm^{-2}) illumination of inverted PDPP5T:IEICO-4F solar cells cast from CF containing 15 vol % CB and 0.2 vol % DIO. Film thickness is ~130 nm. (b) Corresponding EQE spectra measured with bias illumination.

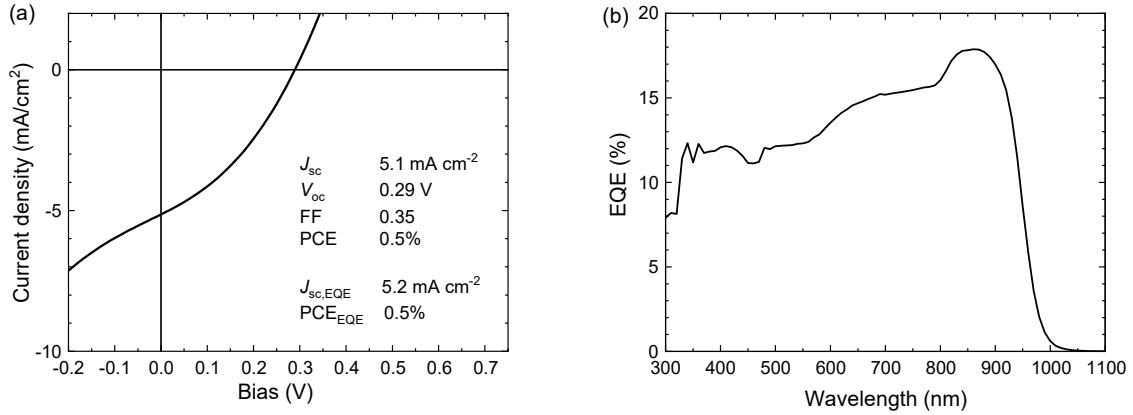

Figure S6. (a) *J*–*V* measurements under simulated AM1.5 G (100 mW cm^{-2}) illumination of inverted PDPP5T:IEICO-4F solar cells cast from CF containing 10 vol % TCE and 0.2 vol % DIO. (b) Corresponding EQE spectra measured with bias illumination.

.

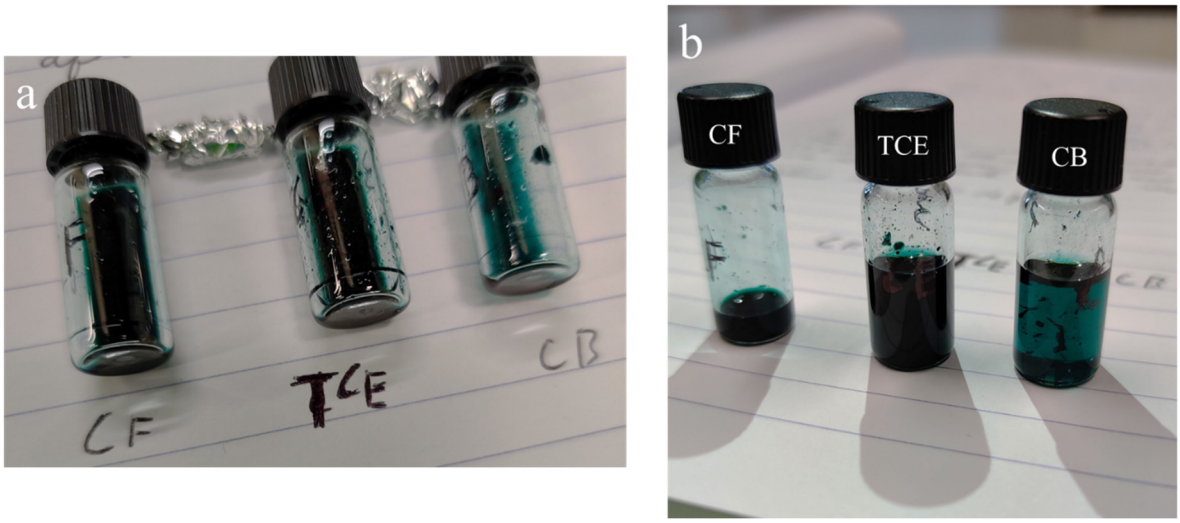

Figure S7. Solubility of PDPP5T in CF, TCE, and CB. (a) Photograph of vials containing 0.5 mg PDPP5T with 200 µL CF, TCE, or CB (0.2 vol % DIO) respectively after heating for 1h at 80 °C. (b) Same after adding 800 µL TCE and CB (0.2 vol % DIO) to these vials.

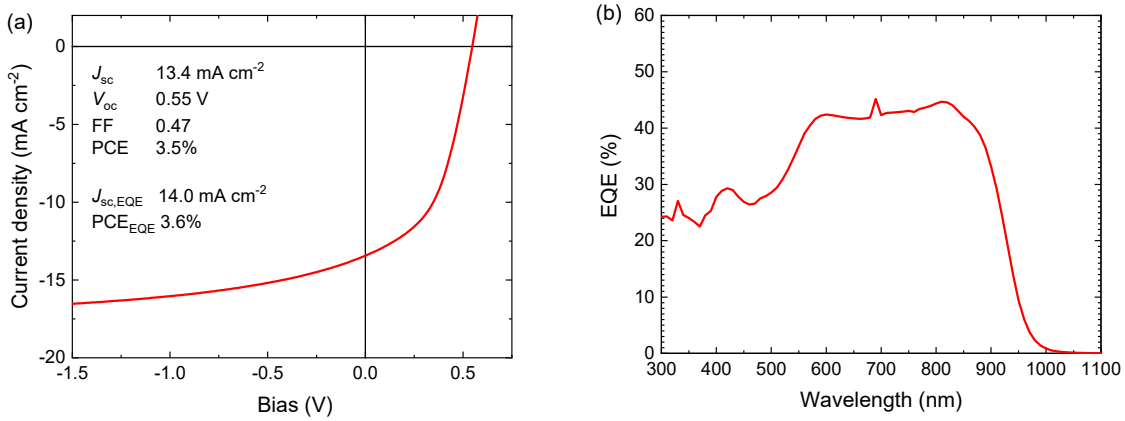

Figure S8. (a) *J*–*V* measurements under simulated AM1.5 G (100 mW cm^{-2}) illumination of regular PDPP5T:IEICO-4F solar cells cast from CF containing 10 vol % CB and 0.2 vol % DIO. Film thickness is ~130 nm. (b) Corresponding EQE spectra measured with bias illumination.

Table S4. Device characteristics for regular PDPP5T:IEICO-4F (130 nm) solar cells cast from a CF:CB mixture.

CB (vol %)	J_{SC} (mA cm^{-2}) [a]	V_{OC} (V)	FF (-)	PCE (%) [a]
10	13.5	0.55	0.47	3.5

[a] J_{SC} determined by integrating the EQE spectrum measured with ~1-sun bias illumination (Figure S8b).

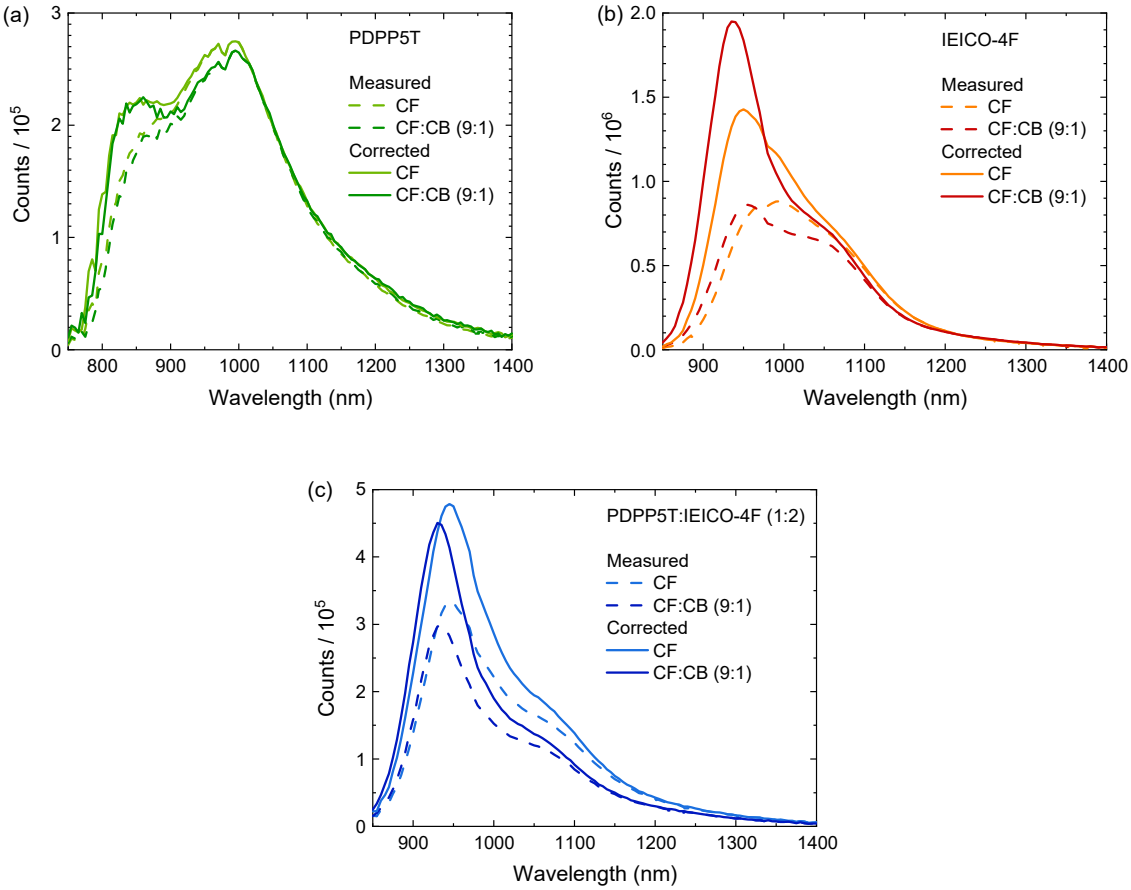

Figure S9. Measured (dashed lines) and corrected (see Note S1) (solid lines) PL spectra of layers cast from CF without and with 10 vol % CB. (a) PDPP5T. (b) IEICO-4F. (c) PDPP5T:IEICO-4F (1:2 w/w).

Note S1. Optical simulations method and protocol

PL correction. Self-absorption and thin film interference significantly influence the measured lineshape in PL. The thin film interference effects stems from the low-quality cavity that is formed when a thin (thickness < coherence length of light) organic layer is deposited on a substrate (glass/quartz) because of the refractive index differences across the interface of air-organic and organic-substrate. This low-quality cavity changes the effective photon density-of-states within the cavity, enhancing the emission (and outcoupling) of some wavelengths from certain depths while suppressing others.

In this protocol (following the work of Dyson *et al.*),[S13] incident light of a given wavelength is considered illuminating the sample at an incident angle. The angle and excitation wavelength used in the physical measurement are to be provided to the simulation. The excitation beam generates an excitation profile within the active layer which is simulated using Setfos 5.0 (FLUXiM) considering thin-film interference effects. Exciton diffusion and

associated broadening/smoothening of the excitation profile are assumed to have little influence in this work.

Next, the wavelength-dependent outcoupling is calculated for every 1 nm depth in the organic layer. This is done by assessing the outcoupled spectra of a spectrally flat emitter at this depth within the organic film (Setfos 5.0, FLUXiM). A point dipole is assumed and S-/P-polarized light is simulated independently and later averaged. The outcoupled spectra are influenced by self-absorption, because light travels through an absorbing organic layer, and by the photon density-of-states altered by the cavity. The outcoupling angle is again determined by the physical measurement and serves as an input variable to the simulation.

Finally, the weighted average is taken of the outcoupled spectra originating from every 1 nm depth. The weight addressed to each depth corresponds to the simulated excitation profile. The resulting spectrum reflects the increase/decrease in PL-outcoupling efficiency at every wavelength as a result of self-absorption and the low-quality cavity, and can be regarded as a wavelength-dependent correction factor. Then the measured spectra are corrected for extrinsic effects by dividing by this factor. This results in the corrected (intrinsic) spectrum of photoluminescence of the organic layer. This intrinsic spectrum facilitates discussion on the photophysical changes within organic layers as a consequence of different processing conditions.

For additional details we refer to Dyson *et al*.[S13]

EL correction. The protocol used for EL correction is a slight adaptation to the one for PL described above. In EL simulations there is no incident light beam and further it is assumed that the generation profile in EL is not depth-dependent. Furthermore, a full solar cell stack is considered, including transport layers and contacts. Especially the opaque back-contact increases the cavity quality and resulting contribution to the outcoupled spectrum.

Ultra-low extinction coefficient. For calculating the (ultra-low) extinction coefficient (k), the method described by Kaiser *et al*.[S14] served as inspiration. Using the script provided by Burkhard *et al*.[S12] as a basis, the fraction of light absorbed by the active layer (F_{abs}) is calculated using the complex refractive index and thickness of every layer as input. Then a wavelength independent internal quantum efficiency (IQE) is determined by dividing the EQE (in the spectral region well above the bandgap) with F_{abs}. Next, the optics in the sub-bandgap region are assessed. The start of the sub-bandgap region was manually defined by judging the shortest wavelength at which the experimental uncertainty in k, determined from variable angle spectroscopic ellipsometry (VASE), was of significant influence. At this wavelength (λ), k was adjusted such that the product of $F_{abs}(\lambda)$ and the IQE matches the sub-bandgap EQE(λ) that was

experimentally determined. In fitting $k(\lambda)$, the k of the previous wavelength (i.e. one wavelength-step shorter, $k(\lambda\text{-}\Delta\lambda)$) was used as initial value and inserted in the script of Burkhard *et al.*[S12] to calculate the $F_{abs}(\lambda)$. Then, the $k(\lambda)$ was varied such that the sub-bandgap calculated EQE(λ) (the product of $F_{abs}(\lambda)$ and the constant IQE) agrees with the measured value. This process is repeated in an iterative manner from short to long wavelengths for every wavelength following the first (shortest) wavelength of the sub-bandgap region. Taking the $k(\lambda\text{-}\Delta\lambda)$ in every step as the starting parameter for fitting, the $k(\lambda)$ of the full sub-bandgap region is determined. This calculated k is exempt of thin-film interference effects stemming from the cavity formed by the solar cell stack and therefore allows for a better discussion of the intrinsic photophysical properties of the blends examined using sub-bandgap EQE.

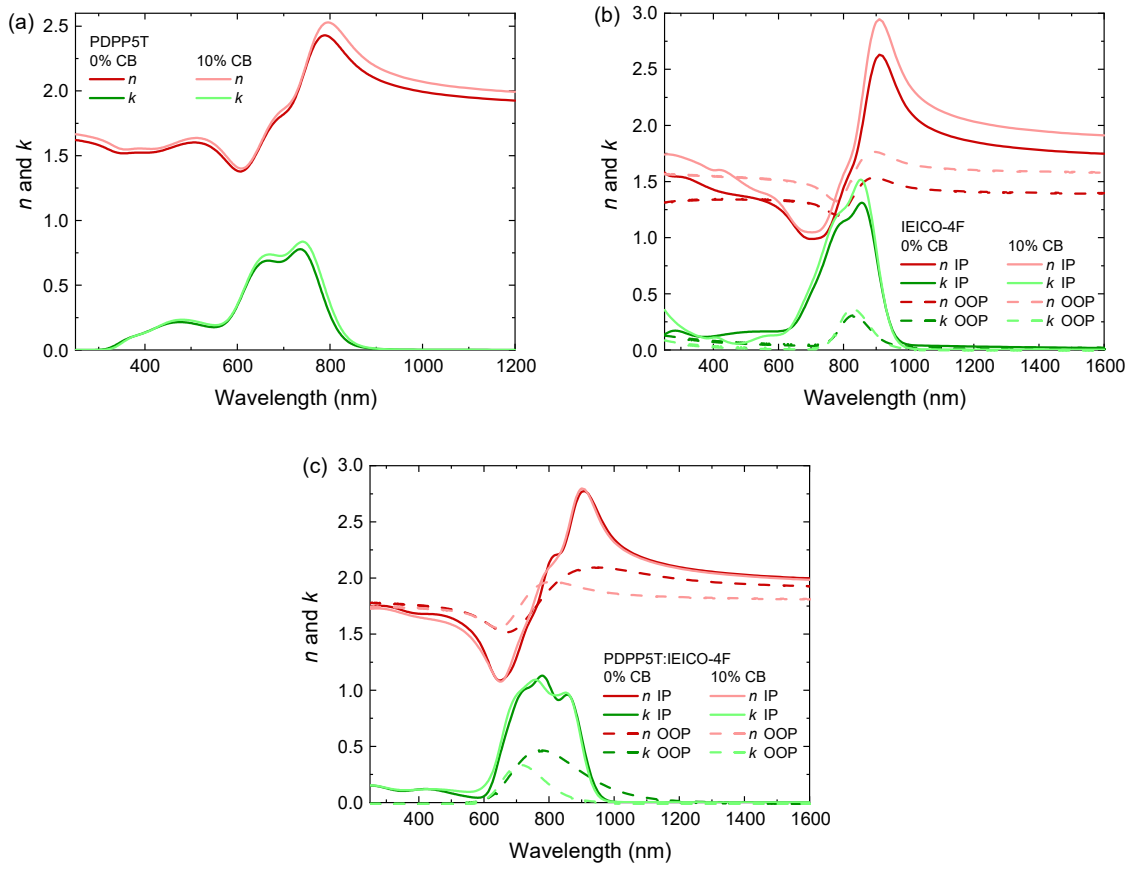

Figure S10. Complex refractive index (n and k) obtained from ellipsometry for layers cast from CF or CF:CB (9:1 v/v). For anisotropic layers in-plane (IP, continuous line) and out-of-plane (OOP, dashed line) refractive indices and extinction coefficients are included. (a) PDPP5T layer. (b) IEICO-4F layer. (c) PDPP5T:IEICO-4F (1:2 w/w) layer.

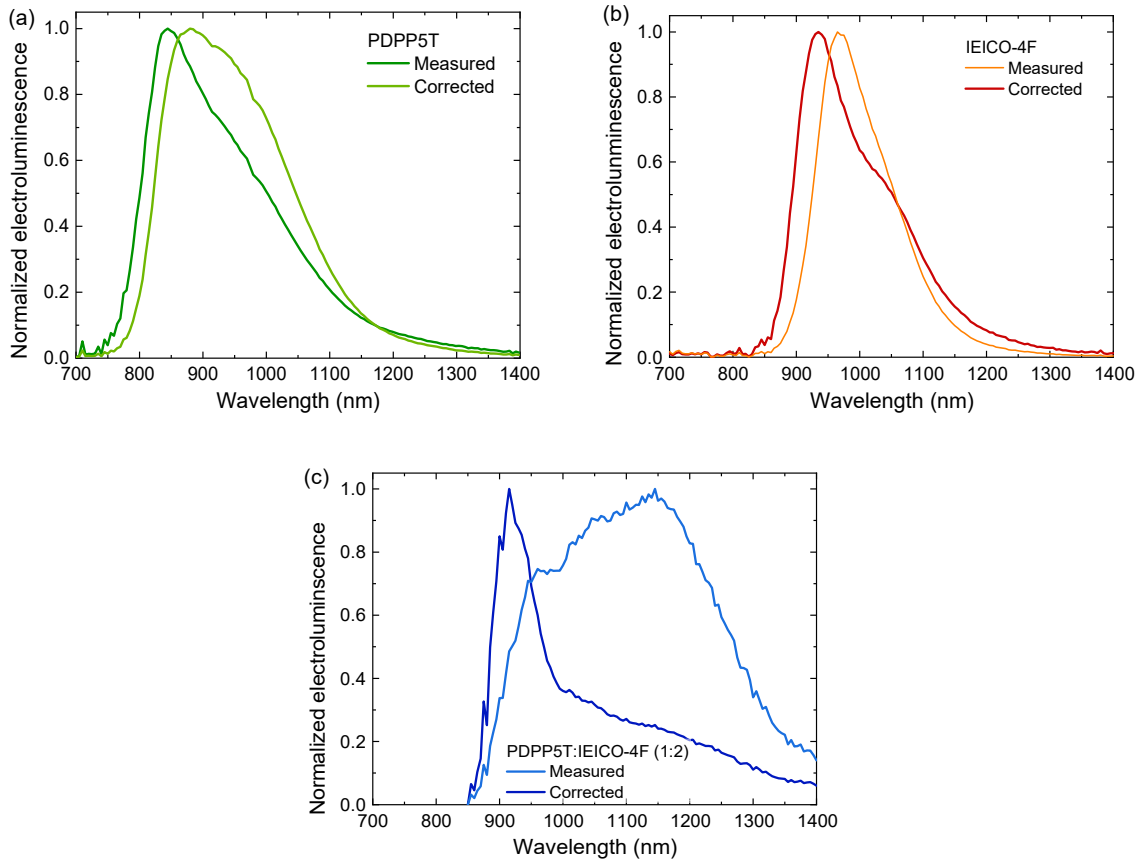

Figure S11. Normalized measured (dashed lines) and corrected (see Note S1) (solid lines) EL spectra of layers cast from CF with 10 vol % CB. (a) PDPP5T. (b) IEICO-4F. (c) PDPP5T:IEICO-4F (1:2 w/w).

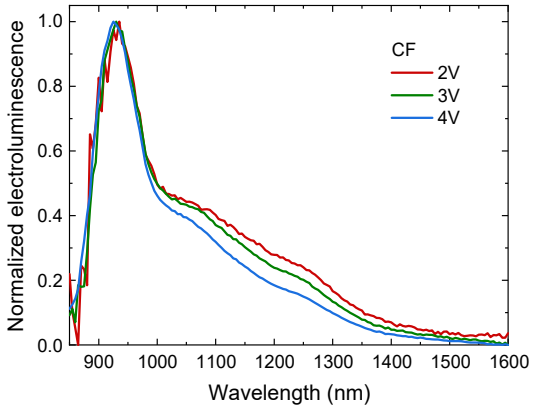

Figure S12. Normalized EL spectra of PDPP5T:IEICO-4F (1:2 w/w) from CF under varying forward bias.

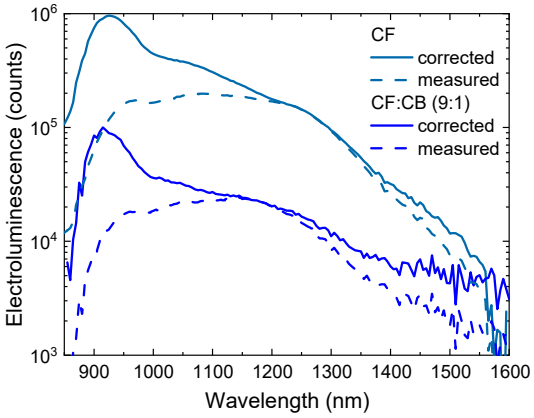

Figure S13. Measured (dashed lines) and corrected (see Note S1) (solid lines) EL spectra of PDPP5T:IEICO-4F (1:2 w/w) layers cast from CF and from CF:CB (9:1 v/v).

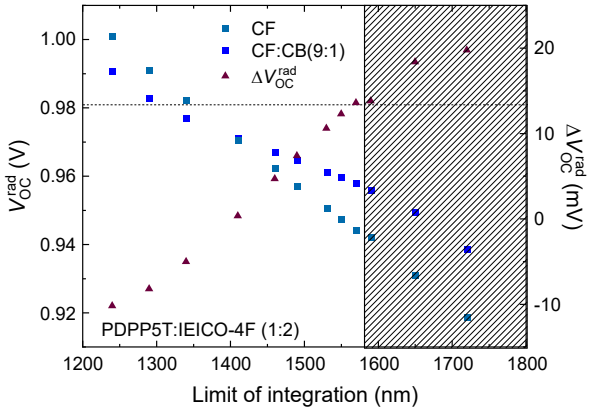

Figure S14. Calculated V_{OC}^{rad} for various integration limits for layers cast from CF and from CF:CB (9:1 v/v) using the EQEs displayed in Figure 4d. The difference in V_{OC}^{rad} between the two cells is given in red (ΔV_{OC}^{rad}) and the noise-level is indicated by the shaded region. The ΔV_{OC}^{rad} near the noise-level was determined to be approximately 13 mV, presented by a horizontal dashed line.

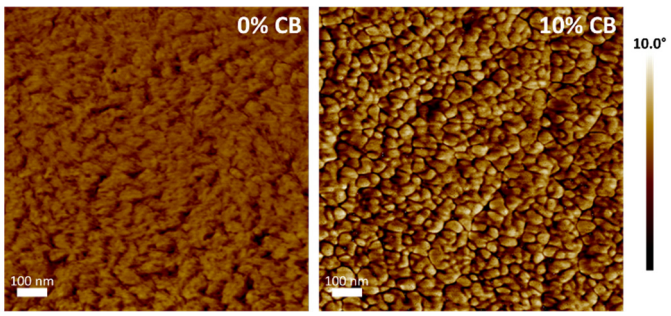

Figure S15. AFM phase images PDPP5T:IEICO-4F films cast from CF (left) and CF:CB (9:1 v/v) (right), corresponding to the height images shown in Figure 5.

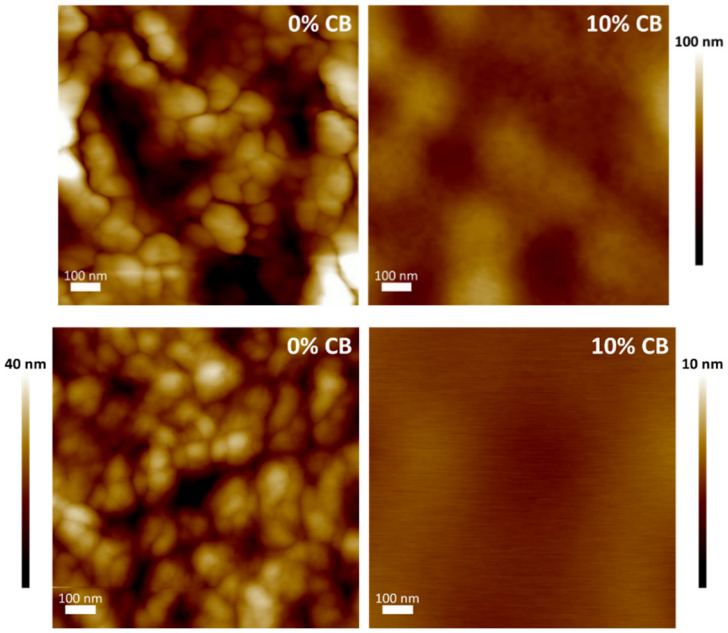

Figure S16. AFM height images of IEICO-4F films cast from CF (left) or CF:CB (9:1 v/v) (right) spin coated at 800 rpm (top, 93 nm and 79 nm respectively) or 2000 rpm (bottom, 45 nm and 58 nm respectively).

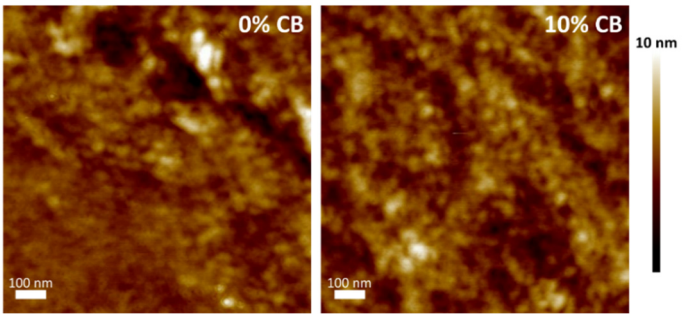

Figure S17. AFM height images of PDPP5T films cast from CF (left) or CF:CB (9:1 v/v) (right) at 800 rpm (41.8 nm and 41.5 nm respectively).

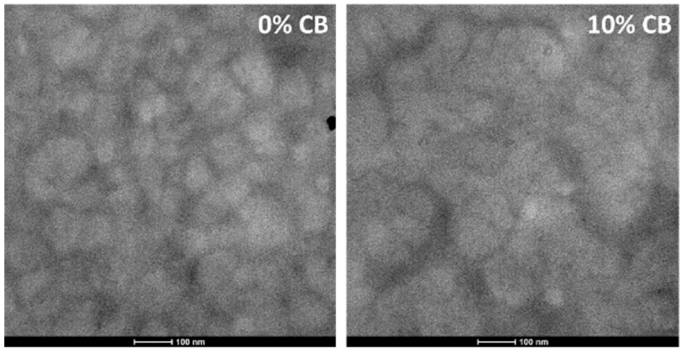

Figure S18. TEM micrographs of PDPP5T:IEICO-4F films cast from CF (left) and CF:CB (9:1 v/v) (right).

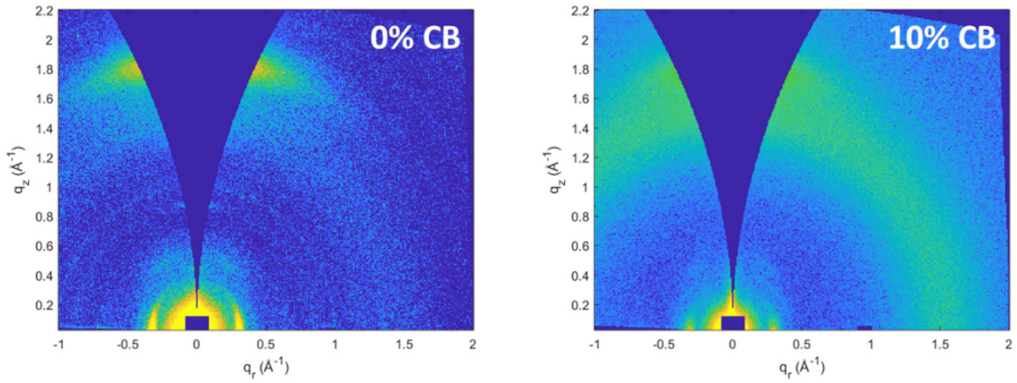

Figure S19. 2D-GIWAXS data on IEICO-4F layers cast from CF (left) or CF:CB (9:1 v/v) (right).

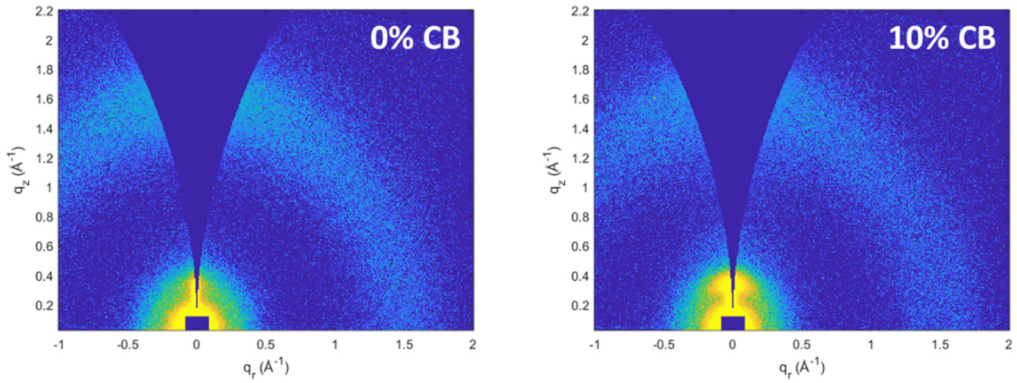

Figure S20. 2D-GIWAXS data on PDPP5T layers cast from CF (left) or CF:CB (9:1 v/v) (right).

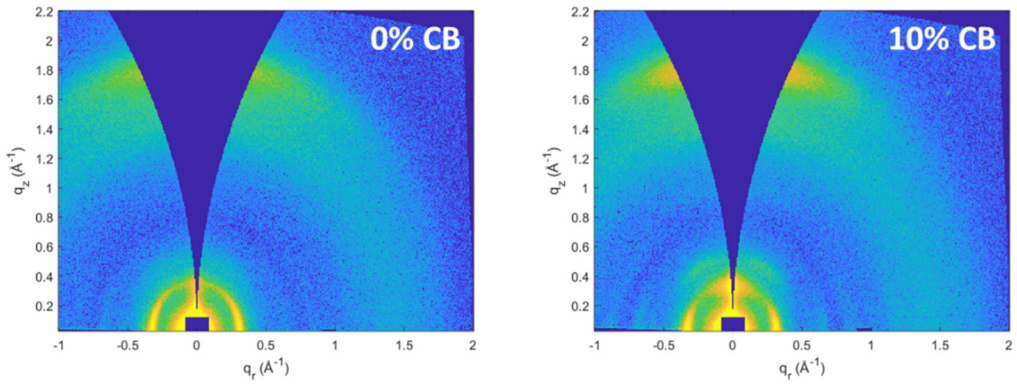

Figure S21. 2D-GIWAXS data on PDPP5T:IEICO-4F layers cast CF (left) or CF:CB (9:1 v/v) (right).

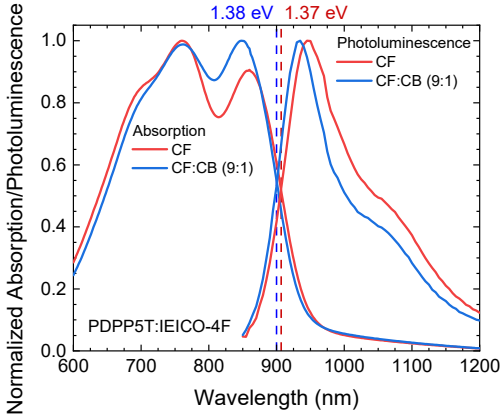

Figure S22. The measured absorption spectra (from Figure 1b) and PL spectra (from Figure S9c) recorded for a layer of PDPP5T:IEICO-4F cast from CF (red) or CF:CB (9:1) (blue). The intersection of PL and absorption is indicated by a dashed line accompanied by a value for the bandgap, determined to be 1.37 eV and 1.38 eV for processing from CF (red) and CF:CB (9:1) (blue) respectively.

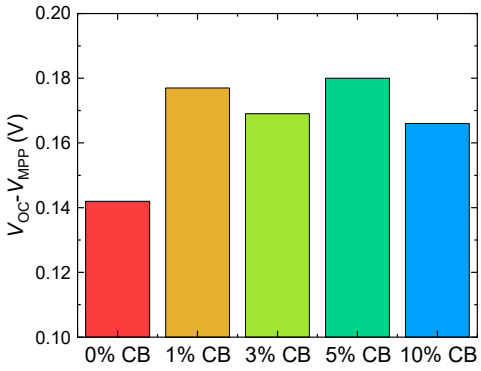

Figure S23. The difference between V_{OC} and the maximum power point voltage (V_{MPP}) for inverted PDPP5T:IEICO-4F solar cells using an active layer (~130 nm) cast from CF with 0, 1, 3, 5, and 10 vol % CB illuminated with ~1 sun light. Corresponding *J*–*V* measurements are shown in Figure 2a.

References

(S1) Negash, A.; Genene, Z.; Eachambadi, R.T.; Kesters, J.; Van den Brande, N.; D'Haen, J.; Penxten, H.; Abdulahi, B.A.; Wang, E.; Vandewal, K.; et al. Diketopyrrolopyrrole-based terpolymers with tunable broad band absorption for fullerene and fullerene-free polymer solar cells. *J. Mater. Chem. C* **2019**, *7*, 3375-3384.

(S2) Pan, L.; Liu, T.; Wang, J.; Ye, L.; Luo, Z.; Ma, R.; Pang, S.; Chen, Y.; Ade, H.; Yan, H.; et al. Efficient organic ternary solar cells employing narrow band gap diketopyrrolopyrrole polymers and nonfullerene acceptors. *Chem. Mater.* **2020**, *32*, 7309−7317.

(S3) Song, X.; Gasparini, N.; Nahid, M. M.; Paleti, S. H. K.; Li, C.; Li, W.; Ade, H.; Baran, D. Efficient DPP donor and nonfullerene acceptor organic solar cells with high photon-to-current ratio and low energetic loss. *Adv. Funct. Mater.* **2019**, *29*, 1902441.

(S4) Jiang, X.; Xu, Y.; Wang, X.; Wu, Y.; Feng, G.; Li, C.; Ma W.; Li W. Non-fullerene organic solar cells based on diketopyrrolopyrrole polymers as electron donors and ITIC as an electron acceptor. *Phys. Chem. Chem. Phys.* **2017**, *19*, 8069–8075.

(S5) Ye, L.; Jiang, W.; Zhao, W.; Zhang, S.; Cui, Y.; Wang, Z.; Hou, J. Toward efficient non-fullerene polymer solar cells: selection of donor polymers. *Org. Electron*. **2015**, *17*, 295–303.

(S6) Li, C.; Zhang, A.; Feng, G.; Yang, F.; Jiang, X.; Yu, Y.; Xia, D. Li, W. A systematical investigation of non-fullerene solar cells based on diketopyrrolopyrrole polymers as electron donor. *Org. Electron*. **2016**, *35*, 112–117.

(S7) Li, C.; Zhang, A.; Wang, Z.; Liu, F.; Zhou, Y.; Russell, T. P.; Li, Y.; Li, W. All polymer solar cells with diketopyrrolopyrrole-polymers as electron donor and a naphthalenediimide-polymer as electron acceptor. *RSC Adv*. **2016**, *6*, 35677–35683.

(S8) Li, W.; Roelofs, W. S.; Turbiez, M.; Wienk, M. M.; Janssen, R. A. J. Polymer solar cells with diketopyrrolopyrrole conjugated polymers as the electron donor and electron acceptor. *Adv. Mater*. **2014**, *26*, 3304–3309.

(S9) Zhang, A.; Wang, Q.; Bovee, R. A. A.; Li, C.; Zhang, J.; Zhou, Y.; Wei, Z.; Li, Y.; Janssen, R. A. J.; Wang, Z.; et al. Perfluoroalkyl-substituted conjugated polymers as electron acceptors for all-polymer solar cells: the effect of diiodoperfluoroalkane additives. *J. Mater. Chem*. *A* **2016**, *4*, 7736–7745.

(S10) Zhang, A.; Xiao, C.; Meng, D.; Wang, Q.; Zhang, X.; Hu, W.; Zhan, X.; Wang, Z.; Janssen, R. A. J.; Li, W. Conjugated polymers with deep LUMO levels for field-effect transistors and polymer–polymer solar cells. *J. Mater. Chem. C* **2015**, *3*, 8255–8261.

(S11) Jung, J. W.; Jo, W. H. A low band-gap copolymer composed of thienyl substituted anthracene and diketopyrrolopyrrole compatible with multiple electron acceptors for high efficiency polymer solar cells. *Polym. Chem.* **2015**, *6*, 4013–4019.

(S12) Burkhard, G. F.; Hoke, E. T.; McGehee, M. D. Accounting for interference, scattering, and electrode absorption to make accurate internal quantum efficiency measurements in organic and other thin solar cells. *Adv. Mater.* **2010**, *22*, 3293–3297.

(S13) Dyson, M. J.; Van der Pol, T. P. A.; Meskers, S. C. J. Extrinsic influences on photoluminescence spectral lineshape in thin films. *Adv. Optical Mater*. **2021**, 2001997.

(S14) Kaiser, C.; Zeiske, S.; Meredith, P.; Armin, A. Determining ultralow absorption coefficients of organic semiconductors from the sub-bandgap photovoltaic external quantum efficiency. *Adv. Opt. Mater.* **2020**, *8*, 1901542.